PROCEEDINGS, 49th Workshop on Geothermal Reservoir Engineering
Stanford University, Stanford, California, February 12-14, 2024
SGP-TR-227

Updated three-dimensional temperature maps for the Great Basin, USA

Erick R. Burns[1], Jacob DeAngelo[2], and Colin F. Williams[2]

[1]U.S. Geological Survey, Portland, Oregon, USA; [2]U.S. Geological Survey, Moffett Field, California, USA

eburns@usgs.gov

Keywords: Geothermal energy resource assessment, heat flow, temperature

1. ABSTRACT

As part of the periodic update of the geothermal energy assessments for the USA (e.g., last update by Williams and others, 2008), a new three-dimensional temperature map has been constructed for the Great Basin, USA. Williams and DeAngelo (2011) identified uncertainty in estimates of conductive heat flow near land surface as the largest contributor to uncertainty in previously published temperature maps. The new temperature maps incorporate new conductive heat flow estimates developed by DeAngelo and others (2023). Predicted temperatures at depth are compared with representative measurements (for conductively dominated conditions), showing good agreement under relatively simple uniform conditions. Inputs included radiogenic heat production for all layers of 1.89 $\mu W/m^3$, effective bulk thermal conductivity of 2.7 W/m/°C for all rocks underlying sedimentary basins, and a previously published (Williams and DeAngelo, 2011) empirically driven estimate of increasing thermal conductivity with depth in sedimentary sequences. The resulting three-dimensional temperature model is published in a USGS data release associated with this manuscript (Burns and others, 2023).

2. INTRODUCTION

The U.S. Geological Survey (USGS) is updating the 2008 assessment of moderate- to high-temperature geothermal resources of the Great Basin (extent shown in Fig 1; Williams and others, 2008). As part of the provisional assessment of Enhanced Geothermal Systems (EGS), the distribution of temperatures shallower than 6 km depth that exceed 150 °C are used to estimate the in situ energy that is available to produce electricity, provided that technologies can be developed to effectively access this heat over engineering timescales of decades. USGS estimated a mean electric power resource on private and accessible public land of approximately 520,000 MWe EGS for the western United States, which is similar to the resource estimate reported by a Department of Energy-sponsored panel convened by the Massachusetts Institute of Technology (Tester and others, 2006). The method of estimating temperatures and associated uncertainty in temperatures is documented in Williams and DeAngelo (2011).

1.1 2008 Heat Flow and Temperature Models

Williams and DeAngelo (2011) provide a comprehensive description of the process of creating three-dimensional temperature maps (temperature is proportional to available heat for electricity) and understanding the cumulative uncertainty associated with choices made during the assessment process. First, maps of heat flow at or near land surface are generated, possibly using multiple competing models to understand uncertainty in predictions under a range of assumptions and interpolation strategies (e.g., smooth regularized splines, ordinary kriging, radial basis functions, etc.). Second, vertical distributions of temperatures are estimated at each location assuming one-dimensional heat conduction. For the preferred model of Williams and DeAngelo (2011), temperature estimates are based on surface heat flow, surface temperature, and vertical distributions of thermal conductivity and radiogenic heat production.

Vertical geology is conceptualized as consisting of basins filled with sediments and semi-lithified sedimentary deposits, underlain with a variety of igneous, metamorphic, and low-porosity sedimentary rocks. Because data are few, analog systems were used to estimate thermal conductivity as a function of depth through the upper sedimentary units (Fig. 2). For rocks underlying the upper sedimentary units, best available information indicates effective bulk thermal conductivities range from 2.4 to 3.0 W/m/°C. Radiogenic heat production for all layers is estimated to be to be a uniform 1.89±0.95 $\mu W/m^3$ (mean ± one standard deviation; Munroe and Sass, 1974) for the upper 6 km of the crust. Thermal conductivity of quartz-rich rocks (i.e., rocks representative of the Great Basin) decreases with increasing temperature, and the relation of Birch and Clark (1940) is used to account for the temperature dependence.

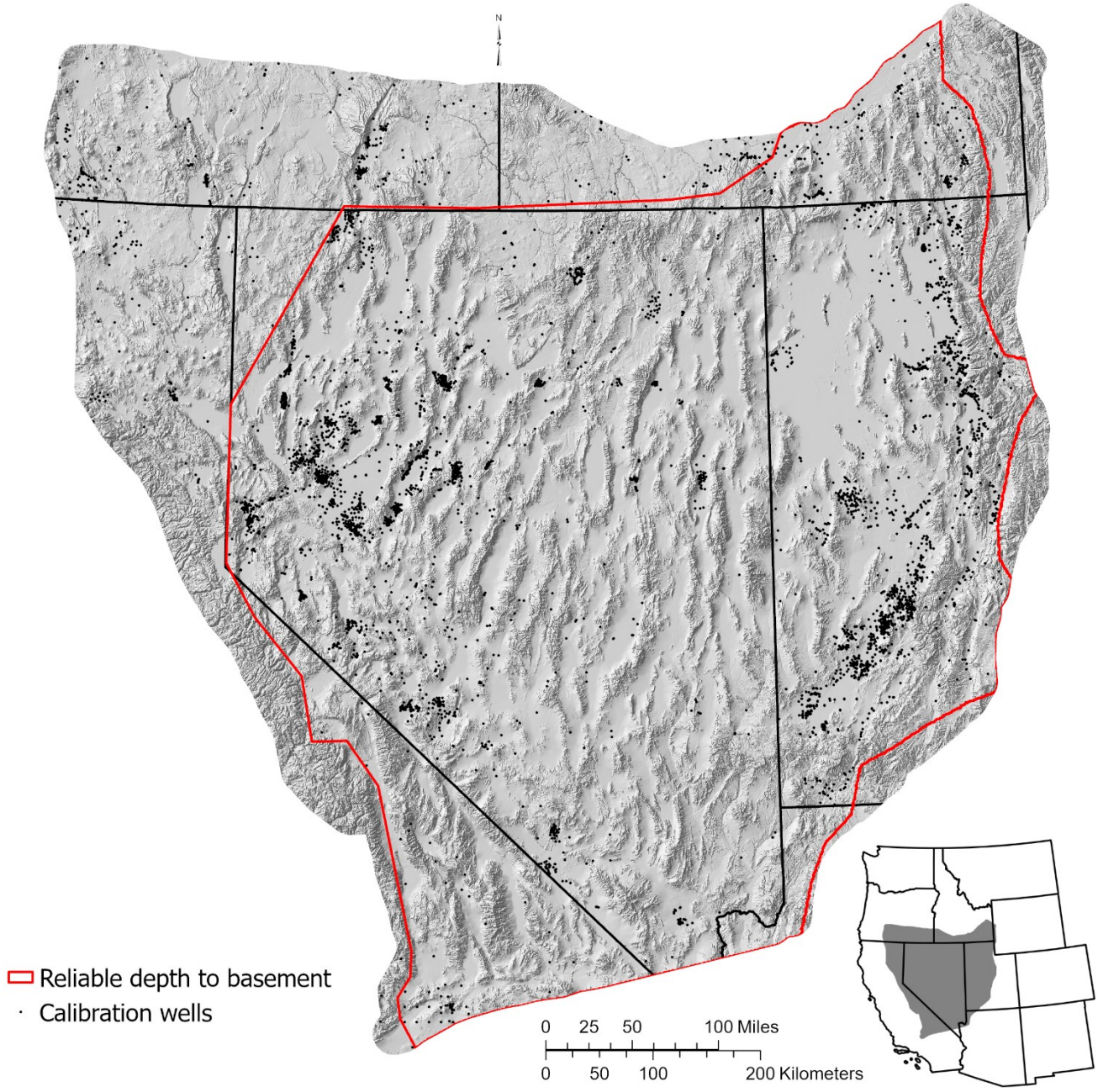

Figure 1: Location map showing the extent of the study area (hillshade [National Atlas of the United States, 2012]), the extent over which the sedimentary thickness is estimated to be most reliable (red outline estimated from Glen and others (2022)), and wells compared with simulated temperatures for calibration.

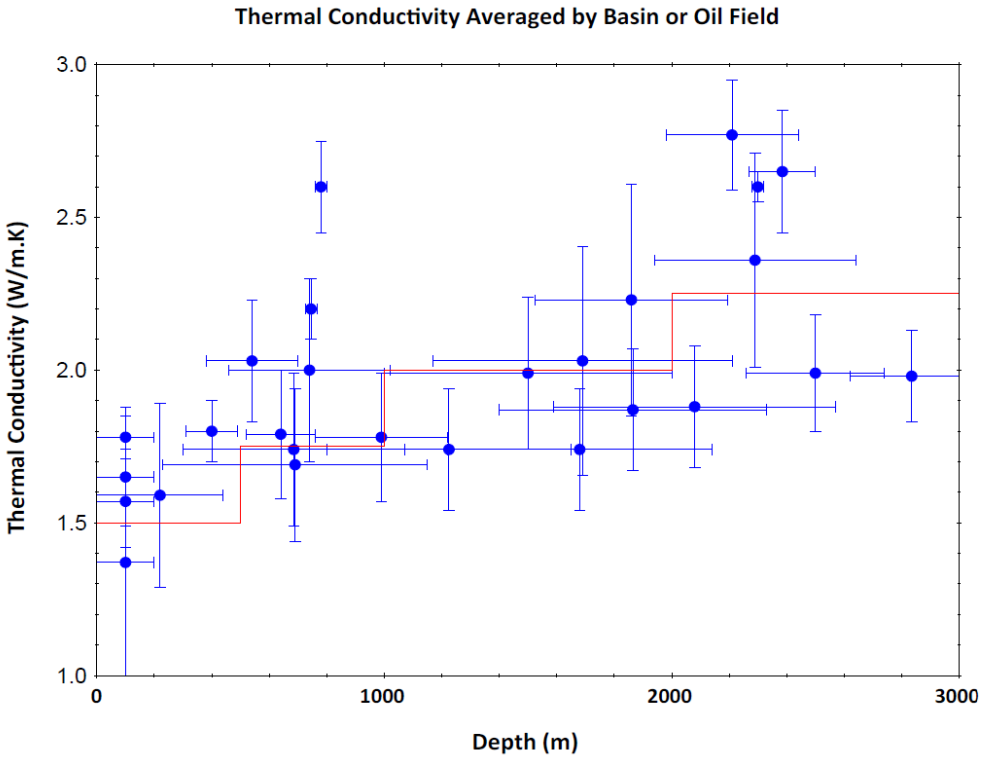

Figure 2: Plot showing the distribution of thermal conductivity with depth for sedimentary basins in California and Nevada (this is Figure 4 of Williams and DeAngelo, 2011). The red line shows the simulated conditions used for sedimentary basins for construction of the three-dimensional temperature map used for estimating EGS resources of the western USA. For the model summarized herein, a constant value of 2.4 W/m/°C (analogous to W/m/°K) is used for depths greater than 3,000 m.

Williams and DeAngelo (2011) state that, "Provided near-surface heat flow measurements are accurate and representative of thermal conditions at the depth of interest, the major source of uncertainty in any model for temperature at depth is the thermal conductivity, which can span a wide range of values due to variations in both mineralogy and porosity (e.g., Clauser, 2006)", but that, given the variable spatial coverage and quality of surface heat flow measurements, of the various factors that affect uncertainty in temperature predictions "the influence of uncertainty in surface heat flow is by far the largest". Uncertainty in thermal conductivity was addressed during resource assessment by making a range of resource estimates across the likely range of thermal conductivity and radiogenic heat production values. Uncertainty in heat flow estimates was evaluated by using the aforementioned range of interpolation strategies, and when available, estimates of error (e.g., the kriging variance). Ultimately, EGS energy resource estimates (and uncertainty) were made by translating the range of heat content estimates into estimates of recoverable heat, assuming a range of thermal recovery scenarios for individual EGS plants and under some plausible regional development scenarios.

1.2 New Heat Flow Maps

DeAngelo and others (2023a) produced new heat flow maps (Figure 3), and a major improvement in these maps is separation of conductive and convective signals, which was accomplished by separating the regional conductive trends from local convective departures (e.g., thermal halos that are a few km across for individual convective upflow zones). The maps used for previous assessments (Williams and others, 2008; Williams and DeAngelo, 2011) represented heat flow with mixed conductive and convective signals, though efforts were made to mitigate the influence of extremely large heat flow measurements (i.e., convective outliers). The temperature model of Williams and DeAngelo (2011) implicitly assumes that the value of surface heat flow is the value of conduction from the shallow subsurface to the surface, so use of the new DeAngelo and others (2023a) maps of conductive heat flow is postulated to improve accuracy and reduce uncertainty in estimated crustal temperatures.

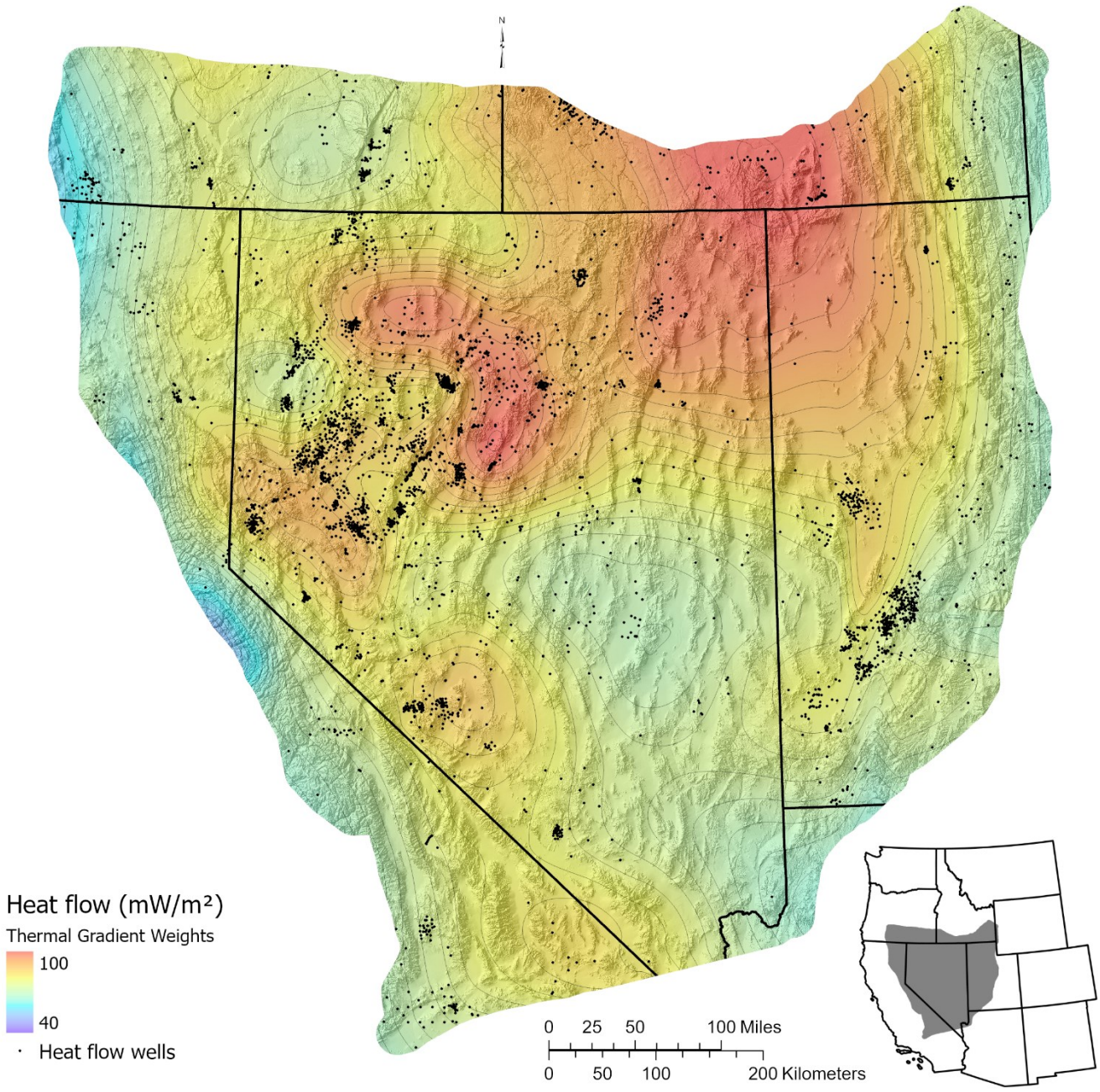

Figure 3: The preferred conductive heat flow map of DeAngelo and others (2023a). Wells shown are those used to calibrate the map. Incorporation of these heat flow estimates is the primary update to the boundary conditions of Williams and DeAngelo (2011), resulting in an updated three-dimensional temperature map. Hillshade derived from USGS National Atlas (National Atlas of the United States, 2012).

3. METHODS

We use the general heat flow model of Williams and DeAngelo (2011) with the new conductive heat flow map of DeAngelo and others (2023a) to construct a new 3D temperature model. Although data are noisy and preferentially sampled from convective parts of the system, we evaluate the heat flow model of Williams and DeAngelo by subsampling bottom-hole temperatures that are within the range of possible conductive heat flow conditions, then identifying where predictions are higher or lower than measured.

2.1 One-dimensional Conductive Heat Flow Model

The model of Williams and DeAngelo (2011) is used to estimate temperature with depth using the new estimates of conductive heat flow by DeAngelo and others (2023a). Conductive heat flow (q) is given by Fourier's Law:

$$\mathrm{q} = \lambda \frac{dT}{dz} \tag{1}$$

where λ is thermal conductivity (W m^{-1} °C^{-1}), T is temperature (°C), and z is depth (m). Increasing temperature with increasing depth yields $\mathrm{q} > 0$, so by the sign convention in equation (1), upward heat flow is positive. Implicit to equation (1) is that heat flow is vertical, so this equation does not strictly apply to locations with non-negligible lateral thermal gradients (e.g., lateral heat flow is <1% of vertical).

Assuming steady-state conditions, negligible convective heat flow, and uniform constant radiogenic heat production with depth (A); conservation of energy yields:

$$\frac{dq}{dz} = \frac{d}{dz}\left[\lambda(\mathrm{T})\frac{dT}{dz}\right] = -A \tag{2}$$

where it is made explicit that $\lambda(\mathrm{T})$ is a function of temperature, given by:

$$\lambda(\mathrm{T}) = \frac{\lambda_0}{a + bT} \tag{3}$$

where λ_0 is thermal conductivity at 0 °C (i.e., thermal conductivity measured in the lab at ambient temperatures near 0 °C [e.g., measured values shown in Fig. 2]), with $a = 1.0$ and $b = \left(0.0024 - \frac{0.0052}{\lambda_0}\right)$.

Given temperature and heat flow conditions at the upper boundary (T_s and q_s, respectively), the temperature profile below this arbitrary boundary is given by (Williams, 1996):

$$\mathrm{T}(\tilde{\mathrm{z}}) = \frac{1}{b}\left[\exp(c_1\tilde{\mathrm{z}} - c_2\tilde{\mathrm{z}}^2 + c_3) - a\right] \tag{4}$$

where $\tilde{\mathrm{z}}$ is depth below the upper boundary where temperature and heat flow are prescribed, and $c_1 = \frac{bq_s}{\lambda_0}$, $c_2 = \frac{bA}{2\lambda_0}$, and $c_3 = \ln(a + bT_s)$.

Solving equation (2) for heat flow with depth increasing below the upper boundary ($\tilde{\mathrm{z}} > 0$) yields:

$$q(\tilde{\mathrm{z}}) = -A\tilde{\mathrm{z}} + \mathrm{q}_s \tag{5}$$

Equations (4) and (5) apply to any geologic layer with uniform reference thermal conductivity (λ_0) and radiogenic heat production (A), and these conditions are consistent with available information for the upper 6-7 km of crust beneath the Great Basin (Williams and DeAngelo, 2011). We assume that the recent conductive heat flow map of DeAngelo and others (2023a) is a good approximation of heat flow at land surface, assigning this value to a depth of zero. We estimate that at a depth of 10 m, temperature is at the annual average air temperature (estimated from the U.S. National Oceanic and Atmospheric Administration [2023]).

Each location in the Great Basin is simulated with a piecewise uniform model using equations (4) and (5). Reference thermal conductivity (λ_0) for the uppermost sediments and sedimentary rock thickness < 3,000 m are estimated from the red line in Figure 2. Rocks underlying the sedimentary units (thickness typically ranging from zero to 5,000 m, with median and mean values for areas with >10 m thickness of approximately 400 m and 700 m, respectively [Saltus and Jachens, 1995]) are assumed to have uniform reference thermal conductivity with likely values ranging from 2.4 to 3.0 W/m/°C (Williams and DeAngelo, 2011) and radiogenic heat production for all layers of 1.89±0.95 μW/m^3 (mean ± one standard deviation; Munroe and Sass, 1974; Williams and DeAngelo, 2011). Because of increasing compaction and lithification with depth, the general trend of Figure 2 is continued by using the low end of the likely range for rocks underlying sedimentary units (2.4 W/m/°C) for sedimentary thicknesses > 3,000 m. Sedimentary unit thickness estimates are taken from Glen and others (2022), which updates the estimates of Saltus and Jachens (1995) where improved data are available. Results from the

Williams and DeAngelo (2011) heat flow model are shown in Figure 4, where the effects of varying properties demonstrate the relative influence of uncertainty across the range of likely values.

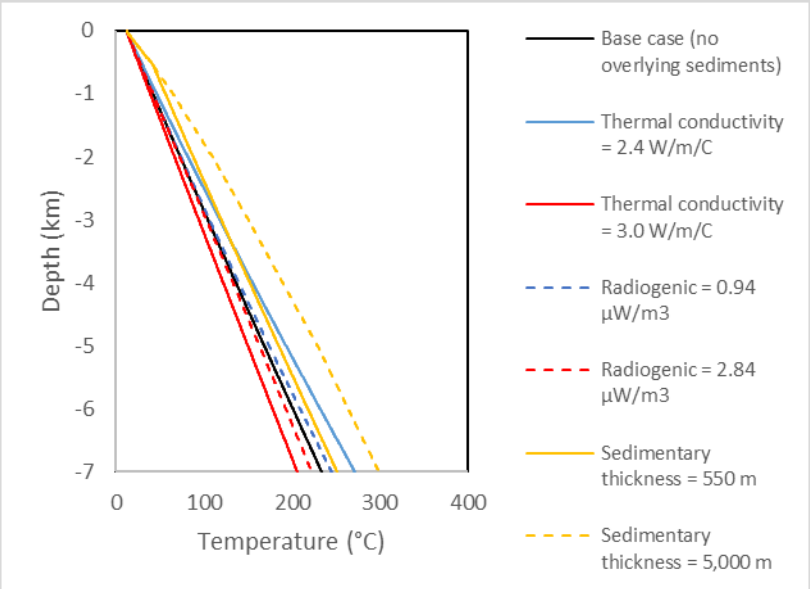

Figure 4: The effects on thermal profiles (computed using equation 4) of varying each property individually across the likely range of values. Base case has zero thickness of sedimentary units, thermal conductivity of 2.7 W/m/°C, and radiogenic heat production of 1.89 µW/m^3. Sedimentary thicknesses represent the deepest basins (5,000 m) and typical thickness of basins (the midpoint between the median [~400 m] and mean [~700 m] thickness of sedimentary basins is 550 m).

For a given heat flow, the insulation effect of sedimentary units is the strongest influence on higher temperatures at depth, and while Figure 4 might imply large lateral temperature gradients (which would result in lateral heat flow), this is mitigated by the topographic effect, where there is a greater thickness of rock above mountains that have little sedimentary thickness (Figure 5). The next strongest influence is thermal conductivity, followed by radiogenic heat production, and these effects can be cumulative (e.g., low radiogenic heat production and low thermal conductivity require a steeper thermal gradient than either of them individually).

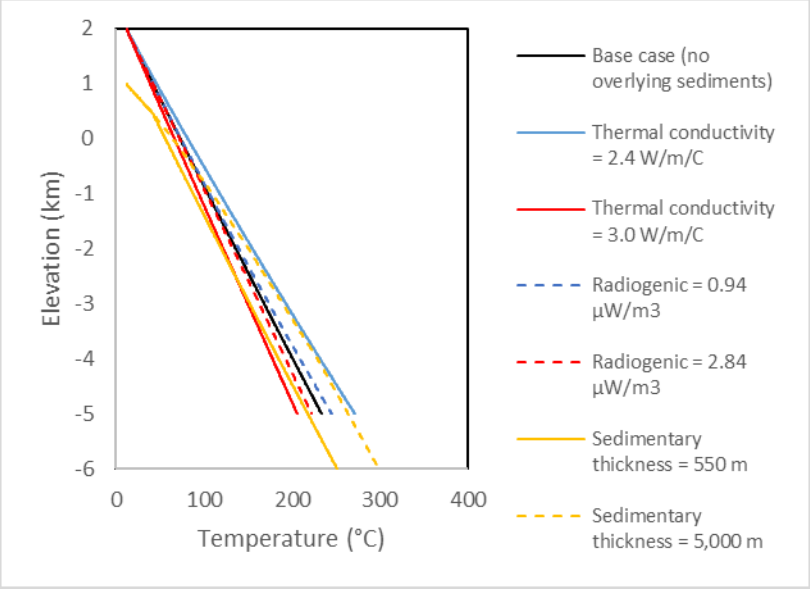

Figure 5: Profiles from Figure 4 corrected for topography. A typical topographic offset of 1-km is assumed (DeAngelo and others, 2023b). Topographic correction shows that horizontal gradients from beneath sedimentary valley are not as large as Figure 4 might imply.

2.2 Temperature Data

Temperature measurements from wells were used to evaluate the estimates of temperature with depth across the Great Basin. Temperature data were collected, curated, and provided by the Great Basin Center for Geothermal Energy (Mlawsky and Ayling, 2020). These data came in the form of data tables that describe well characteristics such as well location, bottom hole temperature and depth, well type (tags: NULL, Groundwater, Geothermal, Stratigraphic, Mining, Oil and Gas), and in some cases measured temperature profiles. Because groundwater wells are likely convectively influenced, they were removed from the set of wells used to evaluate the temperature model, reducing the dataset used from 22,535 to 5,717 wells.

2.3 Evaluation of the model

Available temperature data tend to have been collected preferentially in the vicinity of hydrothermal systems, and therefore, much of these data is not appropriate for use when evaluating the performance of conductive temperature models. However, hydrothermal systems are sparse, likely occupying only a few percent of the total area of the Great Basin; and thermal gradients measured in the near vicinity of hydrothermal upflow show great variability (e.g., DeAngelo and others, 2023a), indicating thermal halos commonly extend for only a few kilometers away from the upflow zone. This limited area of influence implies that even though many measurements represent hydrothermal conditions, there are also temperatures that are representative of the conductive conditions that dominate most of the area of the Great Basin. To find measurements that more likely represent conductive conditions, for any profile (with variable sedimentary unit thickness) with most likely occurring conditions (i.e., 2.7 W/m/°C and 1.89 µW/m^3; Williams and DeAngelo, 2011), measurements should be "near" the resulting profile (Figure 6 shows the base case most likely conditions with zero sedimentary thickness). Near can be defined as being between the upper and lower bounds in Figure 6 (± 7.5 °C/km), with hydrothermal upflow affected temperatures generally being hotter at shallower depths.

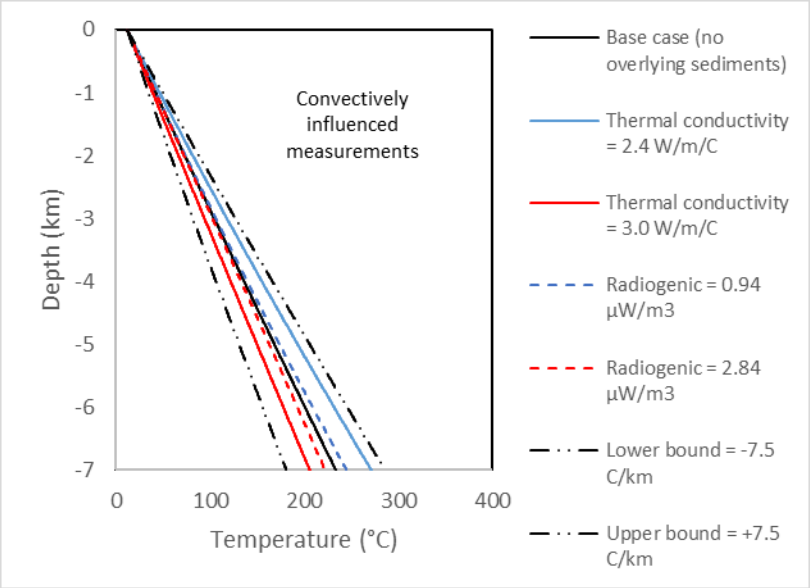

Figure 6: Example profiles with the influence of each property and upper and lower bounds used to identify which measurements are possibly representative of conductive conditions (i.e., between the upper and lower bounds). Convective upflow of heat will result in temperatures higher than the upper bound. Bounds are established in terms of thermal gradient, with the example above showing thermal gradients that are 7.5 °C/km higher or lower than the base case thermal gradient. Temperatures between the bounds could be explained by various combinations of thermal conductivity and radiogenic heating across the range of expected values.

Thermal profiles are generated for all wells with measured bottom hole temperatures, residuals (measured temperature minus model-predicted values) are computed, and measured values within the upper and lower bounds (Figure 6) are used to evaluate model performance. Because the bounds increase with depth, the measure of model performance needs to correct for depth. Recognizing that profiles are nearly straight lines over the depth intervals with measurements, the thermal gradient can be estimated for both the measured value and the predicted value as:

$$measured\ thermal\ gradient \approx \frac{T_{measured} - T_{land\ surface}}{depth} \quad (6)$$

$$predicted\ thermal\ gradient \approx \frac{T_{predicted} - T_{land\ surface}}{depth} \quad (7)$$

The model has good performance if these gradients are the same, so taking the difference between these equations gives the metric of performance of the model used for each measured well:

$$depth\ corrected\ residual \approx \frac{T_{measured} - T_{predicted}}{depth} = \frac{residual}{depth} \quad (8)$$

If a geographic region has depth corrected residuals of zero on average, and there are no strong spatial trends in residual value, then the model is deemed good. If residuals are biased positive for a region, then measured temperatures are higher than predicted, and assuming the heat flow estimate is correct, then thermal conductivity must be lower than currently estimated. Similarly, regions with biased negative residuals would require a higher thermal conductivity to match measurements better. Errors in heat flow estimate, radiogenic heat production, and biased measurements (e.g., bottom hole temperatures not fully equilibrated) may also explain bias, but assuming the new heat flow estimates of DeAngelo and others (2023a) are on average correct and measurement bias is small, varying thermal conductivity across the range of reasonable values for Great Basin geology is a reasonable correction. Ultimately, the purpose of the model is to predict temperature as a measure of stored energy for geothermal energy development, so minor imperfections in model parameters are not likely to be important, if predicted temperatures are generally accurate.

Although the depth corrected residual (Equation (8)) does not depend on land surface temperature, the predicted temperature at depth shifts to the right or left as a function of land surface temperature or the depth to which this temperature is applied (assumed 10-m depth herein). If a vigorously flowing aquifer is present that cools the subsurface to a greater depth, then the thermal profile will be shifted to the left and temperatures will be cooler at depth than are predicted by the current model. As a result, the depth corrected residual is more sensitive to the upper boundary temperature at shallower depths, more easily causing measured temperatures to fall outside the lower and upper bounds (Figure 6), indicating deeper measurements are more reliable for evaluating the model. All wells with bottom hole temperatures between the upper and lower bounds for each borehole (e.g., Figure 6 shows the example with no sediments, but bounds are established well-by-well to account for sedimentary insulation) deeper than 50 m were used for evaluation of the temperature model.

2.4 Construction of 3D temperature map

Following evaluation and calibration of the model, a three-dimensional temperature model is constructed for the Great Basin assuming conductive conditions. A regular 4-km grid of thermal properties (including median sedimentary unit thickness) is used to create a regular grid of one-dimensional thermal profiles. Maps of depth to specific temperature or temperatures at specified depths are constructed by sampling the resulting thermal profiles. Boundary conditions were selected as the median value of each property (i.e., heat flow, land surface temperature, and sedimentary unit thickness) within the extent of the 4-km grid cell.

4. RESULTS

3.1 Evaluation of model fit

Producing the temperature map for thermal conductivity of 2.7 W/m/°C and radiogenic heat production of 1.89 μW/m^3, yields 379 bottom hole temperatures (from the 5,717 wells used) that were from deeper than 50 m and within the upper and lower bounds (±7.5 °C/km) for each of the wells considered (i.e., measurements likely representative of conductively dominated conditions). There were 4,672 wells deeper than 50 m, so 4,293 wells did not fall within the bounds, indicating the vast majority of measurements are likely substantially convectively influenced, which is consistent with most data being collected from researchers targeting hydrothermal zones. The pattern of residuals (Figure 7) shows that on average, the selected thermal properties are a good first-order approximation across the entire Great Basin. Bias would be shown by having regions dominated by red or blue symbols, especially if there were few black dots (lowest error locations) present, but black dots occur uniformly across the study area, and generally, red and blue symbols are well-mixed. Arguably, in western Nevada, red circles are larger than blue dots, indicating either a slightly lower thermal conductivity or slightly higher conductive heat flow may be optimal. A similar argument might be made for other areas, indicating some regionalization of thermal properties, but in general trends in properties are subtle.

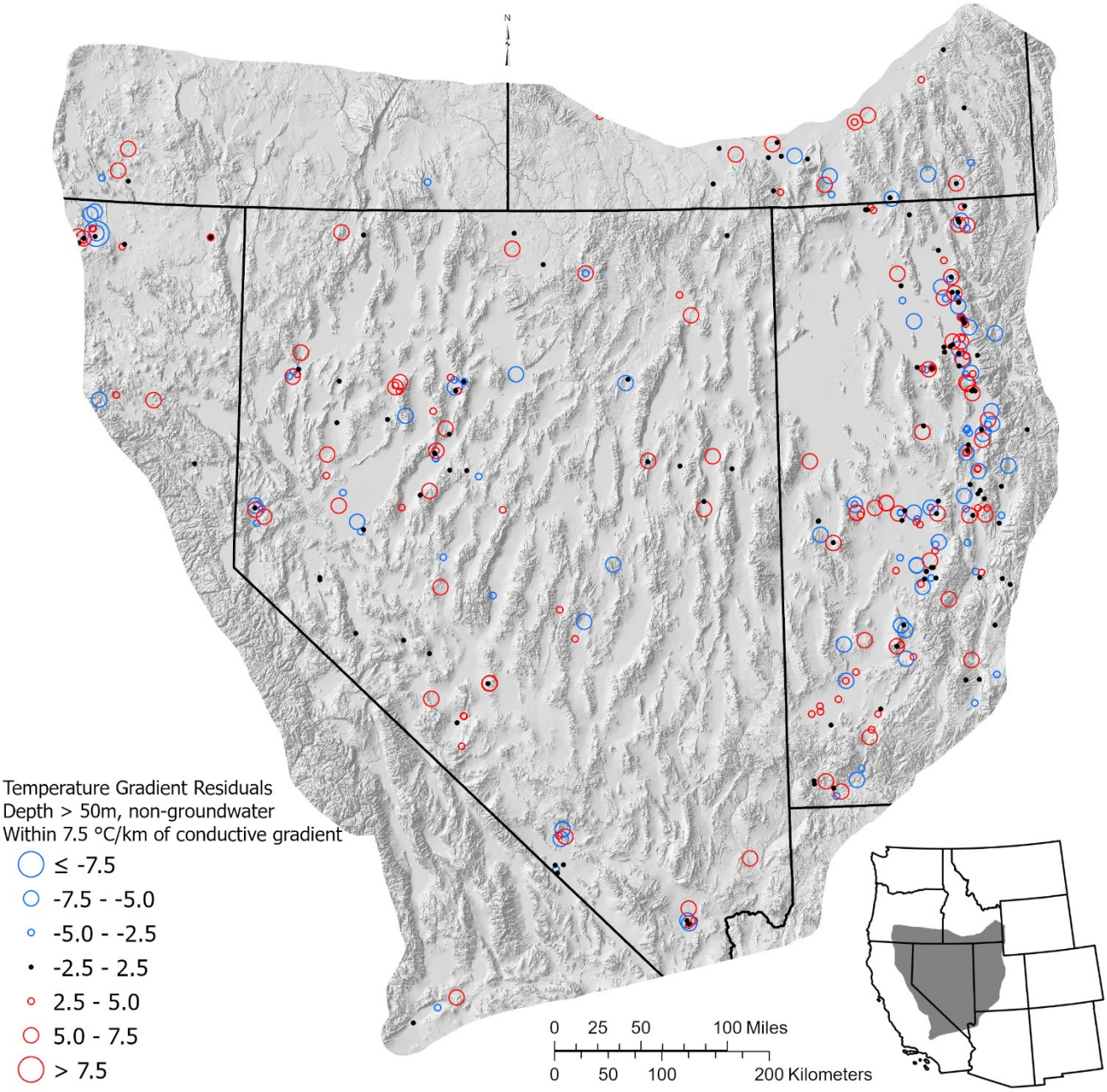

Figure 7: Depth corrected residuals (Equation 8) for the case of variable sediment thickness and thermal conductivity of 2.7 W/m/°C and radiogenic heat production of 1.89 μW/m^3. Hillshade derived from USGS National Atlas (National Atlas of the United States, 2012).

3.2 Three-dimensional temperature grid

Because the new heat conductive heat flow maps of DeAngelo and others (2023a) using the preferred base case values (thermal conductivity of 2.7 W/m/°C and radiogenic heat production of 1.89 μW/m^3; Williams and DeAngelo, 2011) fit the observed temperatures with little if any regional bias, the current best estimate of three-dimensional temperature uses these values (Burns and others, 2023). Uncertainty in these values can be considered in the upcoming EGS assessment for the Great Basin. Temperatures from the grid can be extracted for a range of purposes such as identifying the likely depth to 150 °C (Figure 8). Also provided in the data release are georeferenced grids of temperature at range of depths (i.e., 1, 2, 3, 4, 5, and 6 km) and depth to both the 90 °C and 150 °C isotherm (Burns and others, 2023). Examples are provided in Figures 8 and 9.

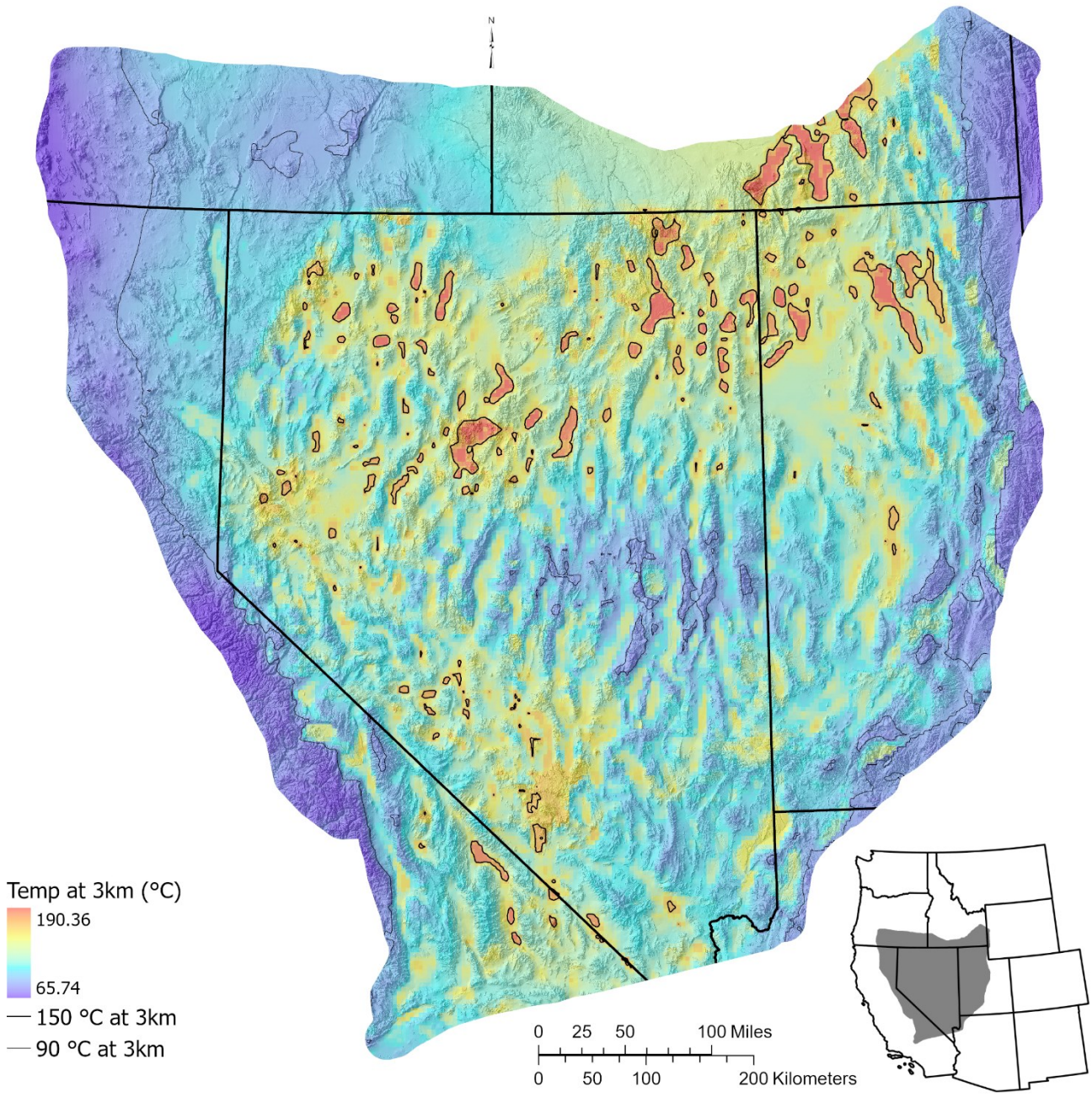

Figure 8: Predicted temperature at 3 km depth (Burns and others, 2023). The 90 and 150 ºC isotherms show that most of the Great Basin is within the 90-150 ºC temperature range at this depth. Hillshade derived from USGS National Atlas (National Atlas of the United States, 2012).

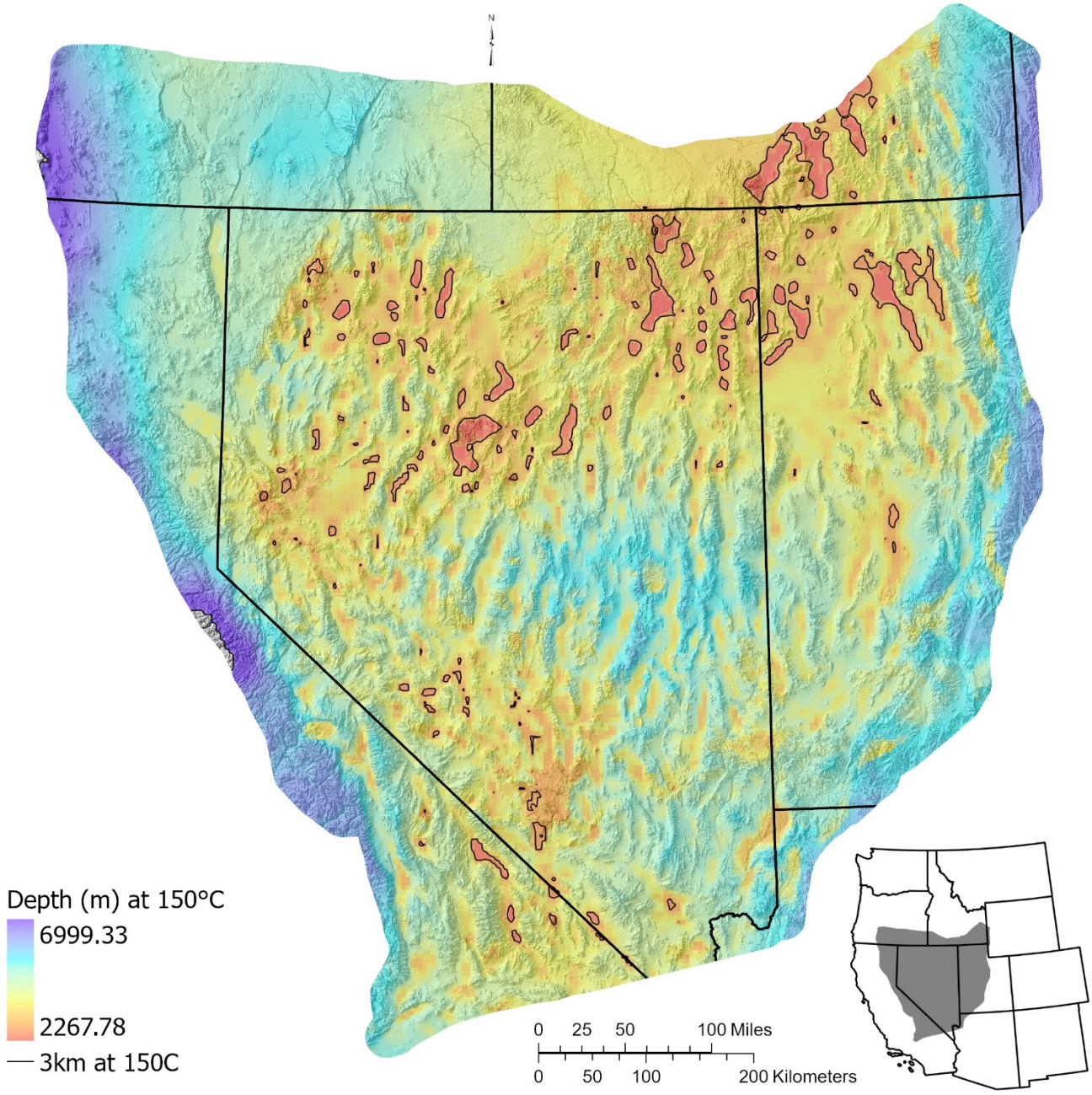

Figure 9: Map of predicted depth to 150 ºC (Burns and others, 2023). The 3-km isobath encloses areas where 150 ºC occur at depths shallower than 3 km (matching the 150 ºC isotherm in Figure 8). For Williams and others (2008), the geology between the 150 ºC surface and 6-km depth were considered viable sources for EGS geothermal electricity production. Hillshade derived from USGS National Atlas (National Atlas of the United States, 2012).

5. SUMMARY

A new three-dimensional temperature map has been created that improves upon previous maps by incorporating new and improved estimates of conductive heat flow. Previous researchers (Williams and DeAngelo, 2011) identified heat flow estimates as the largest source of uncertainty when constructing these temperature maps. The new maps will be used for next-generation EGS assessments of the Great Basin, improving estimates of available geothermal energy and improving understanding of uncertainty associated with these estimates. Because the model that was used to generate the temperature maps assumed conductively dominated heat flow, measured temperatures in areas with substantial deep convective transport of heat will not match predicted values well. However, as long as convective influence

is confined to within a few kilometers of geographically sparse deep hydrothermal circulation zones, estimates for regional energy resources will be reliable.

6. ACKNOWLEDGEMENTS

This study was funded by the U.S. Geological Survey Energy Resources Program and the U.S. Department of Energy - Geothermal Technologies Office under award DE-EE0009254 to the University of Nevada, Reno for the INnovative Geothermal Exploration through Novel Investigations Of Undiscovered Systems (INGENIOUS). Any use of trade, firm, or product names is for descriptive purposes only and does not imply endorsement by the U.S. Government.

7. REFERENCES

1. Burns, E.R., DeAngelo, J., Williams, C.F., 2023, Three-dimensional temperature model of the Great Basin, USA: U.S. Geological Survey data release, https://doi.org/10.5066/P149FR54.
2. Clauser, C., 2006, Geothermal energy, in Heinloth, K., ed., Renewable Energies, Subvol. C, Vol. 3, Group VIII, Advanced Materials and Technologies, Landolt-Bornstein, Springer Verlag, Berlin, p. 480-595.
3. DeAngelo, J., Burns, E.R., Gentry, E., Batir, J.F., Lindsey, C.R., Mordensky, S.P., 2023a, New Maps of Conductive Heat Flow in the Great Basin, USA: Separating Conductive and Convective Influences, Proceedings 48th Stanford Geothermal Workshop, Stanford, California, February 6-8, 2023.
4. DeAngelo, J., Burns, E.R., Lindsey, C.R., and Mordensky, S.P., 2023b, Detrending Great Basin elevation to identify structural patterns for identifying geothermal favorability, Geothermal Rising Conference Transactions, 47, Reno, Nevada, October 1-5, 2023.
5. Glen, J.M.G, Earney, T.E., Zielinski, L.A., Schermerhorn, W.D., Dean, B.J., and Hardwick, C., 2022, Regional geophysical maps of the Great Basin, USA: U.S. Geological Survey data release, https://doi.org/10.5066/P9Z6SA1Z.
6. Mlawsky, E., Ayling, B.F., 2020, GBCGE Subsurface Database Explorer and APIs, data set, retrieved from https://dx.doi.org/10.15121/1987556.
7. National Atlas of the United States, 2012, 100-Meter Resolution Elevation of the Conterminous United States. National Atlas of the United States. Available at: http://purl.stanford.edu/zz186ss2071.
8. Saltus, R.W., and Jachens, R.C., 1995, Gravity and basin-depth maps of the Basin and Range Province, western United States: U.S. Geological Survey Map GP–1012, 1 pl.
9. Tester, J. (Panel chair) and others, 2006, The Future of Geothermal Energy: Impact of Enhanced Geothermal Systems (EGS) on the United States in the 21st Century, Idaho National Lab Report INL/EXT-06-11746, Massachusetts Institute of Technology, Cambridge, Massachusetts, 374p.
10. U.S. National Oceanic and Atmospheric Administration, 2023, U.S. Climate Normals: 1901–2000 Monthly Baseline Mean Temperature data set. Accessed from: https://www.ncei.noaa.gov/products/land-based-station/us-climate-normals on April 24, 2023.
11. Williams, C. F., 1996, Temperature and the seismic/aseismic transition: Observations from the 1992 Landers earthquake, Geophysical Research Letters, v. 23, no. 16, pp 2029-2032, August 1, 1996.
12. Williams, C. F., and DeAngelo, J., 2011, Evaluation of Approaches and Associated Uncertainties in the Estimation of Temperatures in the Upper Crust of the Western United States: GRC Transactions, Vol. 35.
13. Williams, C. F., Reed, M.J., Mariner, R.H., DeAngelo, J., and Galanis, S.P., 2008, Assessment of Moderate-and High-Temperature Geothermal Resources of the United States: U.S. Geological Survey Fact Sheet 2008-3082, U.S. Geological Survey Fact Sheet 2008-3082, pp. 1–4. Available at: http://pubs.usgs.gov/fs/2008/3082/.